

2014-12-30

Thermal Feasibility Analysis of Low Heat Rejection Engine

Peter Johnston Northrop

University of Miami, sales@1016industries.com

Follow this and additional works at: https://scholarlyrepository.miami.edu/oa_theses

Recommended Citation

Northrop, Peter Johnston, "Thermal Feasibility Analysis of Low Heat Rejection Engine" (2014). *Open Access Theses*. 540.
https://scholarlyrepository.miami.edu/oa_theses/540

This Embargoed is brought to you for free and open access by the Electronic Theses and Dissertations at Scholarly Repository. It has been accepted for inclusion in Open Access Theses by an authorized administrator of Scholarly Repository. For more information, please contact repository.library@miami.edu.

UNIVERSITY OF MIAMI

THERMAL FEASIBILITY ANALYSIS OF LOW HEAT REJECTION ENGINE

By

Peter Johnston Northrop

A THESIS

Submitted to the Faculty
of the University of Miami
in partial fulfillment of the requirements for
the degree of Master of Science

Coral Gables, Florida

December 2014

©2014
Peter Johnston Northrop
All Rights Reserved

UNIVERSITY OF MIAMI

A thesis submitted in partial fulfillment of
the requirements for the degree of
Master of Science

THERMAL FEASIBILITY ANALYSIS OF LOW HEAT REJECTION ENGINE

Peter Johnston Northrop

Approved:

Michael R. Swain, Ph.D.
Associate Professor
Mechanical and Aerospace Engineering

M. Brian Blake, Ph.D.
Dean of Graduate School

Matthew N. Swain, Ph.D.
President
Analytical Technologies, Inc.
Miami, Florida

Singiresu S. Rao, Ph.D.
Professor
Mechanical and Aerospace Engineering

Abstract of a thesis at the University of Miami

Thesis supervised by Professor Michael R. Swain.

No. of pages in text (44)

This thesis describes the computational fluid dynamics (CFD) directed analysis used to solve an overheating problem occurring during the warm up period of the crossbred ZKA26 engine in previous research. Internal combustion engine powered generator sets are the primary choice for worldwide operation. Of these generator sets, hardly any use internal combustion automobile engines that are modified beyond the specifications of the manufacturer. These specifications, while well qualified for their intended purpose, are poorly qualified for steady RPM operation as they are used in generator operation. This lack of qualification results in key losses of operational efficiency. This research effort investigates the feasibility of a crossbred engine, previously assembled for the purpose of high efficiency operation for generator use. The engine in question uses a Nissan KA24 block and a Nissan Z20 cylinder head to create a crossbred engine the “ZKA26” with a compression ratio of 14.6:1 and run on a lean mixture of LPG. The chamber surface to volume ratios and heat loss were minimized through the use of hemispherical chambers that lack both squish and swirl areas. The main focus of this study is to investigate and mitigate a failure point in the ZKA26 engine design related to excessive engine block temperatures. Computational Fluid Dynamics was used to find a simulated solution to allow proper engine operation and coolant flow and then experimentally verified with the proposed solutions implemented.

ACKNOWLEDGEMENTS

I would like to thank my advisor and teacher, Dr. Michael Swain. Without his knowledge and guidance this study would not have been possible.

I would also like to thank Dr. Matthew Swain for his aid in both computational and experimental aspects of analysis and design. His time was invaluable in attaining proper CFD modeling to analyze a possible solution.

I would like to thank my parents and family who have support each and every step of this effort and seen the process through to the very end.

TABLE OF CONTENTS

	Page
LIST OF FIGURES	vi
LIST OF TABLES.....	viii
Chapter 1	
Introduction.....	1
Theoretical vs. Practical Limit for Research Conditions	1
Causes of Inefficiency in Real Theory.....	1
Chapter 2	
Previous Work: Background.....	3
Previous Work: 1.6L Genset.....	4
Previous Work: Second Engine	6
Test Condition Philosophy.....	9
Engine Coolant System Restraints.....	10
Chapter 3	
Initial Modeling	13
Solution options	19
Solution Methodology	21
Chapter 4	
Experimental Determination of Water Flow Rate	22
Test Results.....	28
Chapter 5	
Discussion.....	31
Further Work.....	34
APPENDIX A.....	35

APPENDIX B.....	37
APPENDIX C.....	39
APPENDIX D.....	42
REFERENCES	44

LIST OF FIGURES

Figure 1: Flame Speed as a Function of Equivalence Ratio and Material	3
Figure 2: Effect of Turbulence on Combustion	4
Figure 3: Example 2 Spark Plug Head.....	6
Figure 4: Boiling Point of Engine Fluid as a Function of Ethylene Glycol, Temperature and Pressure.....	11
Figure 5: Fluent Mesh Data	13
Figure 6: Fluent Mesh on CAD Solid of Head and Engine Block.....	14
Figure 7: Final Value of the Quality Metric for the Final Chosen Mesh Size	15
Figure 8: Fluent Test Conditions	16
Figure 9: Fluent Advanced Simulation Parameters	16
Figure 10: Fluent Fluid Properties	17
Figure 11: Flow Patterns in Open Thermostat Condition	18
Figure 12: Flow Rate Calibration Apparatus.....	22
Figure 13: Assembled Engine for Flow Rate Calculation	23
Figure 14: Fill Tub for Flow Calculation.....	24
Figure 15: Flow Meter Used for Flow Calculation.....	25
Figure 16: Curve Fit Data of Flow Rate vs. Water Pump RPM	27
Figure 17: Recorded Water Temp of the Two Sides of the Cylinder Block vs. Time.....	28
Figure 18: Recorded Water Temperature vs. Time of Passenger and Drivers Side Thermocouples.....	29
Figure 19: Fluent Figure 1 gal/min Flow	31
Figure 20: Close Up of Hot Spot Location Under 1 gal/min Flow.....	32
Figure A1: CAD Model Passenger Side	35
Figure A2: CAD Model Drivers Side	35
Figure A3: CAD Model Full Driver's Side	36

Figure A4: CAD Model Bottom Side View.....	36
Figure B1: 15 gal/min	37
Figure B2: 17.5 gal/min	37
Figure B3: 20 gal/min	38
Figure B4: 25 gal/min	38
Figure C1: Pulley CAD Back Side	39
Figure C2: Pulley CAD Front Side.....	39
Figure C3: Pulley CAD Side View.....	40
Figure C4: Pulley CAD Back View Dead On.....	41
Figure D1: 16.35 gal/min.....	42
Figure D2: 18.32 gal/min.....	42
Figure D3: 20.27 gal/min.....	43

LIST OF TABLES

Table 1: Previous Work Heat vs. Time Measurements.....	9
Table 2: Water Pump Rpm vs. Flow Rate	26

CHAPTER 1

INTRODUCTION

This thesis describes the Computational Fluid Dynamics (CFD) directed analysis used to solve an overheating problem occurring during the warm up period of the crossbred ZKA26 engine in previous research. It is a well defined trend to use internal combustion engines in generator sets around the globe. They are easily attainable, rather compact in size, and offer fuel flexibility in order to accommodate local conditions. Internal combustion engine generators are the single largest electrical energy source for off-grid emergency energy, especially in critical locations such as hospitals, hotels, and airports to name a few. By increasing the brake thermal efficiency of the engine, a measure of how well an engine converts fuel heat energy to work; both cost and fuel storage mass and volume are decreased, enabling longer running and more sustainable energy sources in smaller spaces.

THEORETICAL VS. PRACTICAL LIMIT FOR RESEARCH CONDITIONS

In internal combustion engines there is both a theoretical and practical limit to the efficiency that can be attained. In theory, 100% efficiency cannot be attained as this notion violates the Second Law of Thermodynamics, however an analysis of Theoretical vs. Experimental comparison can be made given a set of conditions.

In theory an idealized PV diagram is used which assumes that the fuel/air mixture of the engine is instantaneously ignited when the piston is at the top dead center (TDC) position, and instantaneously converts all of that chemical energy from the fuel burning into thermal energy. A theoretical calculation shows that an engine with a 14.6:1 compression ratio, run on Propane, will yield a theoretical efficiency of 62.13% [1].

CAUSES OF INEFFICIENCY IN REAL THEORY

This 14.6:1 compression ratio was chosen as it is the compression ratio of the experimental engine in this research effort. While theory shows that over 60% efficiency should be possible, there is a practical limit that exists due to non-idealized conditions that occur during operation of

the engine. Most typical internal combustion engines will run at approximately 30% BTE and the reasons for this are as follows:

- 1) **Time losses:** Losses in the time it takes to burn the fuel. It is not instantaneous as assumed in theory. One way to decrease these losses is to increase both squish and swirl in the chamber to create turbulence and increased movement of the flame front to burn the fuel more rapidly.
- 2) **Heat losses:** Not all chemical energy is converted into work. No engine truly contains a 100% adiabatic process. Heat losses to the chamber and water jacket are very prevalent and can be increased or decreased depending up on the chamber design and time losses. Heat losses can be minimized with a reduction in turbulence and a small surface area to volume ratio of the combustion chamber.
- 3) A decrease in the ratio of specific heats of the gases (K) as the temperature increases. The more heat that is added to a molecule of a non-monatomic gas, the less available work can be done. This is directly related to the ratio of specific heats $k = C_p/C_v$. The lower this number the less work that can be produced during the compression-ignition-expansion phase. [2]

CHAPTER 2

PREVIOUS WORK: BACKGROUND

The two engines used in this pursuit of high efficiency IC engine design for generators focused on minimizing the three problems above in order to increase efficiency. In both engines, described later in this thesis, leaning out of the fuel-air ratio was used, meaning adding more air to the mixture. While this reduced the power of the engine, it also decreases the ΔT between the fuel/air mixture before and after combustion. This increases the ratio of specific heats of the working fluid. Unfortunately this tactic also increases time losses, as can be seen by the plot below (FIGURE 1), with especially low flame speeds for lean propane (C_3H_8). [3]

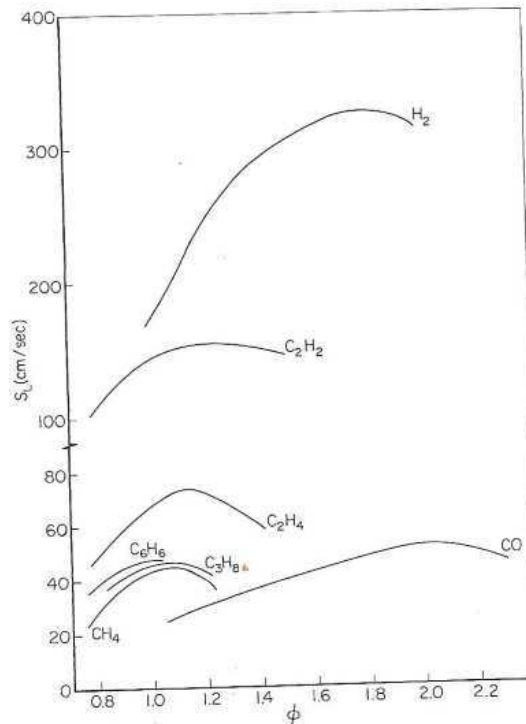


Figure 1: FLAME SPEED AS A FUNCTION OF EQUIVALENCE RATIO AND MATERIAL

Two engines are discussed in this thesis. A 1.6L engine employing squish and swirl and a 2.6 liter engine (this research engine) with the potential to employ multiple ignition sites. The first engine was completed by students Samarajeewa, Seemann and Mackay [4]. The work on the second engine was initiated by Jordan [1]. This thesis continues on this research effort.

PREVIOUS WORK: 1.6L GENSET

Previous work centered upon producing high efficiency, low greenhouse gas emission, EPA compliant genset engines. These engines are to be fueled with propane. The engines were operated with lean air-fuel ratios to increase ratios of specific heat during combustion to increase efficiency. This also simplified minimizing emissions of nitric oxide and carbon monoxide.

Leaning the fuel-air mixture reduces the flame speed which tends to increase unburnt hydrocarbons. To prevent increased levels of this pollutant and to prevent reduced thermal efficiency due to increased time losses the flame speed must be enhanced. The first engine (1.6 liters) increased flame speed by employing swirl and squish.

In the 1.6L genset motor squish and swirl were implemented in multiple different combustion chamber configurations in order to optimize efficiency of the engine by increasing flame speed. This is an approach that permits the use of high compression ratios with ordinary fuels utilizing high turbulence and a compact combustion chamber.

Increasing turbulence reduces knock tendency because combustion occurs more rapidly.

More rapid combustion also increases the range of flammable mixtures as shown below [3]

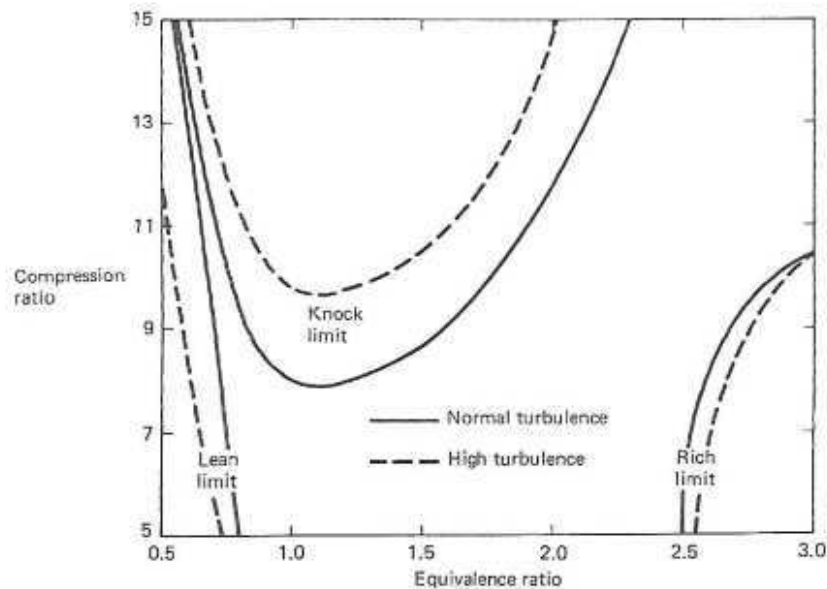


Figure 2: EFFECT OF TURBULENCE ON COMBUSTION

The two main sources for turbulence investigated in the first engine are squish and swirl. Squish is formed when the clearance between part of the cylinder head and piston at the end of the compression stroke is very small. In this area gas is ejected into the main volume of the combustion chamber and the turbulence from this jet increases combustion rate. Using squish will reduce the susceptibility to knock since the gases in the chamber have less time to auto ignite. However, if excessive squish area is used the combustion will become too rapid and noisy and cause reduced efficiency and higher unburnt hydrocarbons. Furthermore, another disadvantage to excessive squish is that it increases airflow velocity against the chamber walls and causes increased heat transfer and reduce thermal efficiency [3].

Swirl on the other hand is created by two factors: by valve design and by intake port design. The design utilizes a shape that creates gas rotation around the axis of the cylinder during the intake stroke that will last through the compression stroke. In swirl designed engines, the inlet tracts tend to be almost horizontal, with slight convergence. The reduction in volume during compression causes an increase in swirl ratio and further reduction of volume causes swirl to break up into turbulence. This enables lean air/fuel ratios to be burnt, giving good fuel economy and low emissions. If swirl is produced, kinetic energy increase for the flow is made at the expense of a reduction in volumetric efficiency. [3]

In the first engine, while a very high compression ratio was attained and very high efficiency of 38% as well, there was a large amount of thermal losses into the water jacket. These losses were of the magnitude 50% and were a direct result of use of the very large squish and swirl to decrease time losses. Thus, while high efficiency was attained, a more effective method to reduce time losses might be found that resulted in less heat losses.

PREVIOUS WORK: SECOND ENGINE

After the analysis of the heat loss in the first engine, it was decided to investigate the use of multiple ignition sites to increase combustion rate, hopefully with a large enough decrease in heat losses to improve thermal efficiency. The work of Oliver Jordan produced a crossbred Nissan 2.6L engine with the ability to be modified for multiple ignition sites. The engine did not require expensive or difficult to obtain components. It employs a hemispherical combustion chamber with low surface to volume ratio. The most important aspect of the second engine is that it provides for reduction of heat losses, and the ability to be drilled and tapped for a second spark plug. [1]



Figure 3: EXAMPLE DUAL SPARK PLUG HEAD

The significance of this feature is that it allows two ignition sites inside one chamber. Whereas the first engine used squish and swirl to increase turbulence, this second engine affords a solution without enhanced turbulence. High swirl rates can quench or distort the flame kernel immediately after the spark plug discharges. To avoid

this the center of swirl must be located near the spark at ignition. With the second engine flame fronts could be initiated from both sides of the chamber creating two flame fronts instead of one. This not only served to minimize the time losses, but it also helped to lower heat losses associated with turbulent burn techniques such as squish and swirl which increase gas velocity at the chamber wall increasing the heat transfer coefficient at the wall. Most other heads that were investigated would have required substantial work to add an additional spark plug, requiring material addition through welding in order to attain the same result. Adding material would affect the chamber shape and could ultimately cause head deformation as well. Thus, the Nissan Nap-Z engine cylinder head was chosen for the second engine.

While, the Nap-Z head is well suited for this project, the Nap-Z block is extremely hard to acquire as they are over 25 years old, meaning replicating these engines would be difficult and potentially expensive. The eventual choice for the block was the “KA” block which can be found inexpensively in most junk yards. This block is also less bulky and has a more efficient design with less friction. The reduction in friction is due to smaller bearing diameter. [5] This was accomplished even with a 40% increase in horsepower for the KA block over the Nap-Z block. The KA head however employs 3 valves per cylinder and does not allow for the second spark plug to be added. Fortunately the KA block and Nap-Z head have the same bore spacing and the thesis **FEASIBILITY STUDY OF A LOW HEAT REJECTION GENERATOR SET ENGINE** sought to determine whether or not this crossbred engine set could overcome the following difficulties:

- 1) **Integrity of the camshaft lobes:** During the design of the engine the camshaft was machined to reduce lift by 47%. This means that the camshaft lobes were machined past their hardened surface, making them susceptible to wear during break in from the rocker arm pushing down on them with the force of the springs. The spring pressure was reduced because the maximum operating rpm was reduced by 60%. Additionally since the lobes were shorter they potentially would not dip into the oil that sits under the camshaft to produce sufficient lubrication. If the softer surface either couldn't withstand the reduced load from the weaker valve springs or did not achieve proper lubrication, then failure could occur during initial break in.
- 2) **Oil Pump:** The stock KA oil pump may not provide sufficient oil pressure for the new crossbred configuration. If this indeed were the case, the engine would not stay properly lubricated and failure would occur. This could occur due to different oiling patterns between the Z head and the KA block. The solution to this problem, should it occur was the use of a different oil pump.
- 3) **Fuel Distribution in each cylinder:** The crossbred engine utilized a modified stock intake manifold that has the coolant passages on the bottom of the manifold removed to optimize gas temperatures entering the cylinder. With no heat being added to the fuel, a higher ratio of specific heats was achieved, together with increased volumetric efficiency and increased knock tolerance. The ZKA26 manifold features no pre-chamber (as in the first engine) so cylinder-to-cylinder air/fuel ratios may vary and lower efficiency. This lower efficiency would be the result of necessitating a richer mixture than desired to maintain proper fuel to each cylinder chamber.

4) Temperature Distribution in the engine: The KA and Nap-Z family of engines have different coolant flow patterns. Water enters the driver side of the block in the KA family of engines while entering on the passenger side in the Nap-Z family of engines. This has the potential to create a situation in which the coolant doesn't properly flow through one side of the block to the other side between the cylinders and into the cylinder head. Three thermocouples and three analog temperature gauges were installed in the second engine order to monitor this process.

TEST CONDITION PHILOSOPHY

The results of previous operation of the crossbred ZKA26 engine with no ethanol glycol or high pressure cooling system showed that 2 of the 4 potential problems were sufficiently solved. The oil pump provided no lower than 40 psi of pressure, sufficient for this motor, an analysis of the cam lobes after running the motor showed no sign of improper wear, but there was an addressable problem of cylinder to cylinder fuel/air ratio variation as shown by the exhaust gas temperatures in the table below.

Time (Minutes)	1	2	3	4	5
Exhaust Port #1 (°F)	N/A	N/A	1239	N/A	N/A
Exhaust Port #2 (°F)	1144	1185	1213	1217	N/A
Exhaust Port #3 (°F)	1160	1203	1214	1213	N/A
Exhaust Port #4 (°F)	1080	1166	1187	1193	N/A
Water Inlet (°F)	79.2	97.1	103.8	117.3	N/A
Right Side Block (Coolant) (°F)	87	137.9	159.7	193.4	N/A
Left Side Block (Coolant) (°F)	78.6	92.6	106.3	128.2	N/A

Table 1: PREVIOUS WORK HEAT VS TIME MEASUREMENTS

There was however one of four problems that became apparent very quickly, the cooling of the engine block.

After two minutes of running the engine, there was a 45.3 degree Fahrenheit difference between each side of the block, and a 65.2 degree Fahrenheit difference at four minutes. At 4 minutes the temperature had increased up to 193 degrees Fahrenheit and the fuel to the engine was shut off. It was noted the coolant water boiled for two short bursts within 1 to 2 seconds after the fuel was shut off, indicating that the temperatures exceeded 212 degrees Fahrenheit.

ENGINE COOLANT SYSTEM RESTRAINTS

In an effort to prevent excessive cooling to the front of the number one cylinder in an inline engine, the water flow from the water pump is offset to one side of the cylinder block or the other. If the water pump is in-line with the center of the front of the cylinders, the first cylinder will be impacted with cool water, consequently creating a cool spot on the front side of the number one cylinder. This process will cause that cylinder to expand unequally and cause uneven wear of the piston rings inside the cylinder. This can lead to blow by past the rings and allow oil to enter the combustion chamber, which increases the unburnt hydrocarbons and can lead to conditions that increase the difficulty of meeting EPA standards.

In the case of the ZKA26 (Second engine) the cylinder head originated on an engine which had the water flow directed down the passenger side of the engine block while the cylinder block used for the ZKA26 engine had the water flow directed down the driver's side of the engine. This difference in block design produced a large enough temperature gradient within the coolant passages of the cylinder block to allow the

condition described above. The postulation was that the short boiling after the fuel shut off was due to the heat already within the metal of the cylinder wall prior to fuel cut off. It is of importance to note that the coolant system of the test engine is not pressurized to 14 psi as an automobile coolant system would be; meaning it is more susceptible to boiling at lower temperatures. Furthermore there was no mixture of glycol in the water. As such the engine is much more susceptible to boiling of the coolant liquid as shown by the figure below.

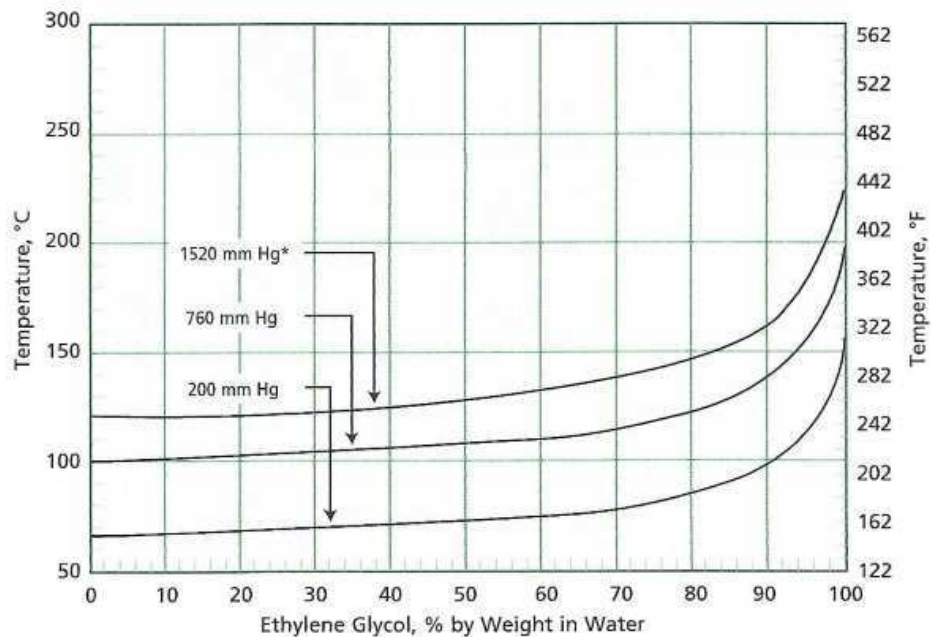


Figure 4: Boiling point of engine fluid as a function of Ethylene Glycol, Temperature and pressure

From the figure above we can see that at 760 mmHg and 0% Glycol the boiling point is 212 °F, whereas under normal car operating conditions of 1520 mmHg and 50% Glycol the boiling temperature is in the neighborhood of 262 degrees. This leaves a 40 degree difference between our test condition and standard operating conditions. Glycol and a pressurized radiator could be used as potential “solution”; however there would be

no solution in the inherent temperature gradient issue between the two sides of the block. This, as mentioned before could lead to wear related issues over time. By creating a solution under the more stringent of conditions there is an opportunity to find a solution to the inherent problem as opposed to the symptom of the problem.

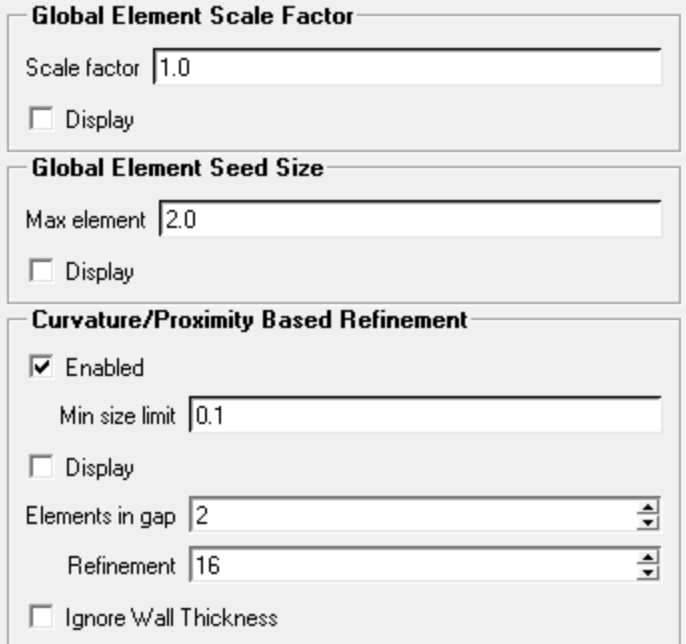
A solution to the problem could be to open the water jackets on the intake manifold and open new holes in the head gasket. This would require additional machine work. The Initial CFD modeling data from this investigation indicated an alternative solution.

CHAPTER 3

INITIAL MODELING

A systematic approach of computer modeling was undertaken in order to accurately assess the overheating condition as seen during physical testing. A 3D CAD model was constructed of the ZKA26 engine block, head gasket, and cylinder head as shown in APPENDIX A

Once the CAD drawings were complete, the completed model in CAD was exported for CFD testing into ICEM CFD and solved with the ANSYS FLUENT SOLVER. The mesh was created using ICEM CFD which gives a lot of control over the mesh and sizing. Parameters can be set to increase your mesh quality, especially for complex geometries. A mesh was created using the following sizing parameters (Figure 6) yielding 490000 elements



The image shows a screenshot of the ANSYS FLUENT MESH DATA dialog box, which is used for configuring meshing parameters. The dialog is organized into three main sections:

- Global Element Scale Factor:** This section contains a text input field for the "Scale factor" set to 1.0, and a checkbox for "Display" which is currently unchecked.
- Global Element Seed Size:** This section contains a text input field for the "Max element" size set to 2.0, and a checkbox for "Display" which is currently unchecked.
- Curvature/Proximity Based Refinement:** This section is expanded and contains several options:
 - A checked checkbox for "Enabled".
 - A text input field for "Min size limit" set to 0.1.
 - A checkbox for "Display" which is currently unchecked.
 - A spin button for "Elements in gap" set to 2.
 - A spin button for "Refinement" set to 16.
 - A checkbox for "Ignore Wall Thickness" which is currently unchecked.

Figure 5: FLUENT MESH DATA

The surface of the mesh is shown in the following figure. It shows the different sizing as the shape of the water jacket changes. The elements in gap in the previous figure make the mesh have at least 2 elements between each gap which is needed for the very small passages between the bottom and top of the water jacket. The curvature and proximity refinement was used in order to adapt the mesh to the thicknesses of the passages in different parts of the jacket.

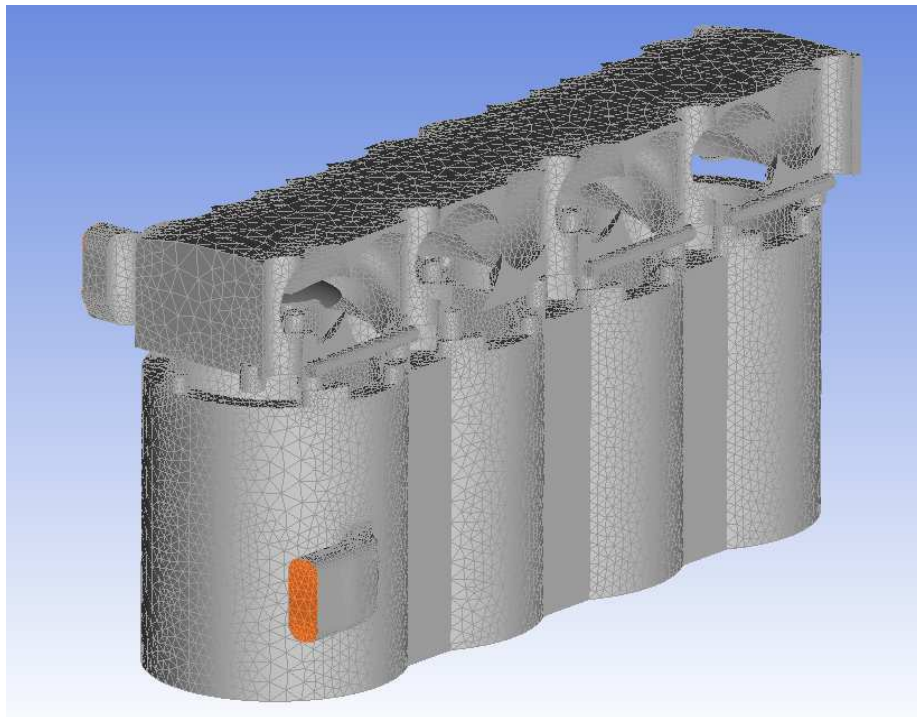


Figure 6: FLUENT MESH ON CAD SOLID OF HEAD and ENGINE BLOCK

Once the mesh is generated in ICEM, extra steps needed to be taken to check and increase the mesh quality if needed. This includes looking at the quality with different metrics and one of those metrics is skewness of elements. ICEM reports the skewness of elements as a ratio of width to length of the tetrahedrals. Anything under 0.10 is considered bad skew and anything under 0.20 is generally not recommended. It is

however very hard to eliminate all elements under 0.20. The following plot shows the final value of the quality metric for the final chosen mesh size.

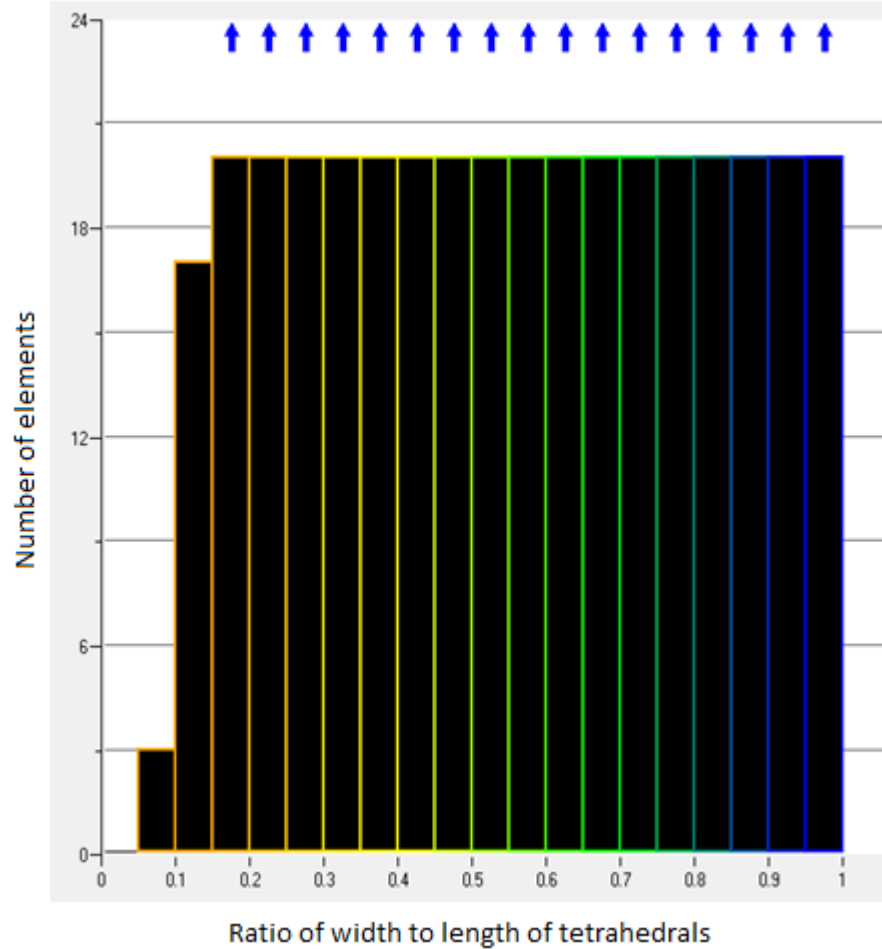


Figure 7: Final value of the quality metric for the final chosen mesh size

Once the mesh was complete, it was loaded in a Computational Fluid Dynamics software known as FLUENT. This CFD software solves equations for mass, momentum and turbulence in each control volume. [6] A pressure based solver was used to solve the flow equations. All the conditions were translated from the actual experimental setup. A steady state simulation of the flow was run.

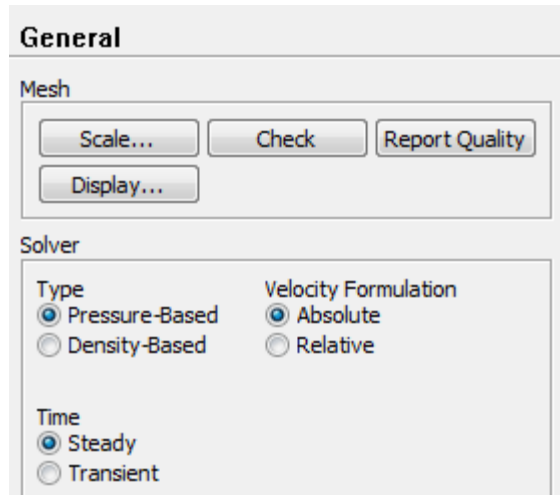


Figure 8: FLUENT TEST CONDITIONS

The viscous model for the fluid flow used was realizable k-epsilon with standard wall function which was used in previous similar tests. The energy is CN for the testing meaning the energy is taken into account and being solved during the simulation of the flow.

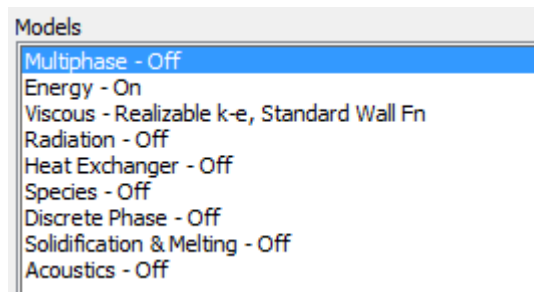


Figure 9: FLUENT ADVANCED SIMULATION PARAMETERS

The fluid used for the flow inside the cylinder was water with the following properties

The screenshot shows the 'FLUENT FLUID PROPERTIES' dialog box. It is divided into several sections:

- Name:** water-liquid
- Material Type:** fluid
- Chemical Formula:** h2o<l>
- FLUENT Fluid Materials:** water-liquid (h2o<l>)
- Mixture:** none
- Order Materials by:** Name (selected), Chemical Formula
- Buttons:** FLUENT Database..., User-Defined Database...
- Properties:**
 - Density (lbm/ft³):** constant, 62.31351
 - Cp (Specific Heat) (btu/lb-r):** constant, 0.9988798
 - Thermal Conductivity (btu/h-ft-r):** constant, 0.3467607
 - Viscosity (lbm/ft-s):** constant, 0.0006739848

Figure 10: FLUENT FLUID PROPERTIES

The solution methods used are shown below. 1st order simulations solutions were used for the testing at different flow rates. The second order results didn't show any appreciable change in the calculation of the flow therefore it was decided to use the less time consuming 1st order analysis.

Inside the FLUENT program we were able to select appropriate inlet and the appropriate outlet which allowed for the same flow pattern as the test engine. The computer modeling was run at 15 gal/min initially based upon reference data calculations as shown below.

What the flow analysis showed as was the complexity of the flow directions inside of the motor. As can be seen from the figure above, there are six separate and distinct flow patterns on the passenger side of the motor. The flow is represented by the vectors, corresponding in velocity to the colors on the left side of the chart. As can be seen the four blank spaces in the figure represent the four combustion chambers of

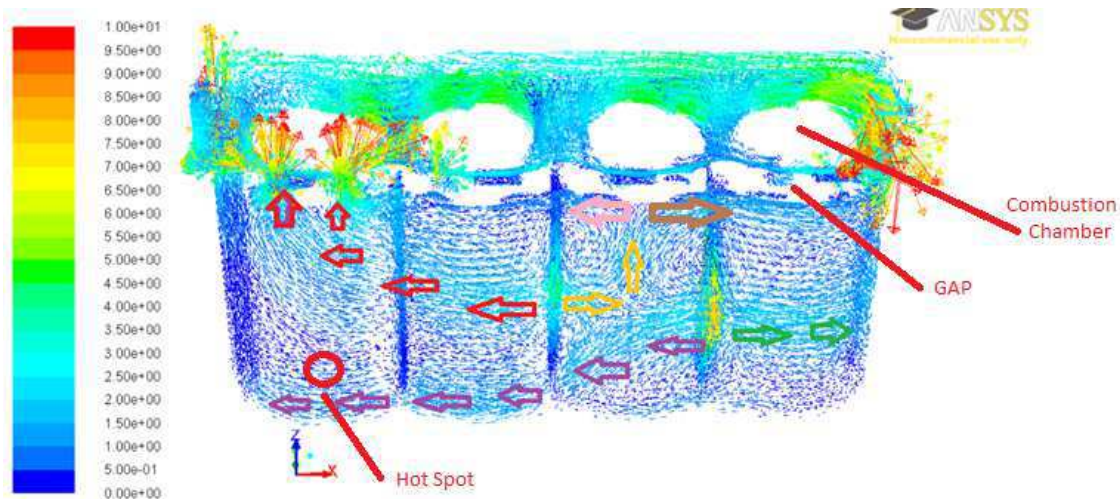


Figure 11: FLOW PATTERNS IN OPEN THERMOSTAT CONDITION

the engine. Similarly a gap is formed by metal between the bottom four cylinders and head as well.

The vector portion of the figure represents flows inside the head, while those in the four cylinders below the gap represent flow in the water jacket surrounding the cylinders, including flow in between the cylinders. As can be seen, the largest velocities are shown in the top left of the figure going vertically, which are the spaces in the head gasket where flow is allowed to move from the engine block to the cylinder head. Drawn on top of the FLUENT vectors are four colored patterns of arrows representing the six generalized flow directions created by running a flow of 15 gal/min through the engine.

As can be seen by the purple and green vectors, the flow passes around the driver's side of cylinder number one and then passes from the driver's side to the passenger side in the water jacket between cylinder one and two. The flow then continues past the passenger side of the bottom of cylinders two and three and eventually around the back of cylinder four. This means that the flow reaching the hot spot (figure 11) on the engine has been heated by three cylinders before reaching that point. Furthermore, from the orange and red arrow sets it shows that between cylinders two and three the flow

splits yet again and heads towards the top of the block, skipping over the location of our hot spot. Thus the only flow moving past the hot spot of the engine is represented by the purple arrow set. This flow visualization clearly explains why a hot spot exists on the passenger side of cylinder number four and leads to the conclusion that a change in flow pattern could be beneficial in providing adequate cooling of the engine to eliminate the overheating issue noted in previous work.

SOLUTION OPTIONS

In order to choose the most appropriate solution, all 4 options were investigated:

- 1) Changing head gasket
- 2) Drilling new holes in the head.
- 3) Changing Intake manifold outlets
- 4) Increasing the water pump speed by modifying the pulley.

From the complexity of the flow patterns of the initial model it was likely stable flow patterns would be a function of inlet velocity. This meant altering the flow patterns by adding and subtracting water passages between the cylinder head and block and would likely create new hot spots as water was redirected to provide additional cooling of an existing hot sport. As such increasing the flow rate of the water pump would increase flow rate of all locations so the problem of low velocity in the front of the block would not become more severe. The initial modeling in FLUENT was run at 15 gal/min, 17.5 gal/min, 20 gal/min, and 25 gal/min which was a range suitable to what the stock pump actually operates within. The resulting images are shown in APPENDIX B.

From the images we can see that at 17.5 gal/min the hot spot location showed increased velocity over the 15.0 gal/min flow pattern of the engine. This was further enhanced with increasing speed of the water pump.

During further investigation of the location of low velocity within the cylinder block, it was noted that the lowest velocities in the main passages were found on the front and back side of the engine, and the lowest flow rate between cylinders was between the third and fourth cylinder. This flow pattern, represented by the purple arrows in figure 11, requires the water that cools the hot spot to travel past three and a half cylinders before cooling the hot spot location. Heat transfer occurring during this circuitous path with low flow raises the water temperature and inhibits heat transfer at the hot spot. From figure 11, we can see that all of the available holes were opened on the back side of the motor already. Machining new openings or changing the head gasket would have minimized effect on changing the condition of low velocity on the bottom of the back side of the motor, and thus, with our FLUENT modeling we were led to consider changing overall water flow rate as a possible solution to the temperature gradient existing in the coolant system.

SOLUTION METHODOLOGY

In order to increase the flow rate by increasing the speed of the water pump, a larger ratio between the crankshaft and water pump pulleys needed to be achieved. This had 3 possibilities:

- 1) Increase crank pulley size (with dampener)
- 2) Decrease pulley size of water pump
- 3) Combination of 1 and 2

There is a dampener on the crankshaft pulley that would be hard to replicate so it was not chosen as the first possible solution. There was also a clearance issue between the water pump and crankshaft pulley if the crankshaft pulley was increased in size.

Machining a new smaller water pump pulley was an effective way to increase water pump speed. The pulley is held to the water pump impeller with four bolts. A CAD drawing of 2 different sized pulleys, both smaller than the factory pulley was made. The first pulley was designed to increase the ratio by 12% (i.e. spin the pump 12% faster). The second pulley was made to be the maximum physically allowable reduction in the water pump pulley diameter which was 24%. Figures of these two pulleys are found in APPENDIX C.

CHAPTER 4

EXPERIMENTAL DETERMINATION OF WATER FLOW RATE

The original values used for the fluid modeling were based on educated guesses as to the water velocity based on the original KA24 engine coolant requirement. To verify our results from the modeling it was necessary to verify the actual speed of the water flowing from the pump.

An experimental reconstruction of the important components of the cooling system (Figure 12+13) was assembled to verify that our estimation range was correct in the first round of FLUENT modeling. The separate engine test apparatus was set up consisting of a bare block, engine cylinder head, intake manifold, front cover, water pump, and thermostat housing as shown below.



Figure 12: FLOWRATE CALIBRATION APPARATUS



Figure 13: ASSEMBLED ENGINE FOR FLOW RATE CALCULATION

In order to obtain results, a tub (Figure 14) was fed with water by three hoses at a rate such that it always kept the tub overflowing. This set the water pressure head at the inlet. A radiator hose (black) identical to the test engine was submerged in this tub and attached to the water pump inlet. The outlet on the intake manifold had a similar radiator hose attached (per the original test setup in the lab for previous results) and measurements were recorded with an EW-32900-82 Flow meter with a range of flow rates from 5 to 35 Gallons per. The flow meter calibrated well at both 10 gal/min and 20 gal/min (this was appropriate as our test range was from 15 to 25 gal/min for FLUENT analysis) when fitted with the third of the machined PVC pipes (Figure 15). It was necessary to make three different PCV sections in order to obtain the most accurate calibration on the scale. The first two attempts did not yield as high accuracy as the final

designed PVC pipe. Calibration was done by positive displacement. The water was brought to an identified gal/min value on the gauge and then for one minute water was fed into a glass container mounted on two scales. The change in weight after one min was converted to volume in order to determine how much water had entered the aquarium during that time. This was then compared with the value shown on the flow meter and found to be within 2% error.



Figure 14: FILL TUB FOR FLOW CALCULATION



Figure 15: FLOW METER USED FOR FLOW CALCULATION

In order to power the water pump, a modified electric grinder motor was mocked up with a modified pulley and variostat in order to adjust RPM to produce rates of 10, 15, and 20 gal/min. The RPM of the water pump at these flow rate values was recorded using a strobe timing light which was accurate to within +/- 1 RPM. It is of note that there were 2 sets of results for 20 gal/min as two different lengths of hose were used on the inlet and outlet designated “short” and “long” which represented both lower and higher levels of friction as the actual engine apparatus in order to determine the effect, if any, on the experimental flow results. Using a T student test to compare the mean values of the two data sets indicated there was a 43.6% chance that the long hose data is the same as the short hose data, thus indicating negligible error from this portion of the apparatus vs. the test engine setup in the lab. Each test was repeated 6 times for accuracy and the results of the data flow collection were as follows:

Run #	10 gal/min long house RPM	15 gal/min long hose RPM	20 gal/min long hose RPM	20 gal/min short hose RPM
1	1469	2139	2915	2873
2	1412	2195	2846	2891
3	1454	2182	2873	2824
4	1431	2169	2852	2867
5	1435	2174	2902	2880
6	1448	2140	2870	2851
Mean	1441.5	2166.5	2876.3	2864.3

Table 2: WATER PUMP RPM VS FLOW RATE

From the ratio of pulley diameters between the crankshaft pulley and the stock water pump pulley, at 1800 RPM on the crankshaft the stock water pump was running at 2340 RPM. From the results above simple math followed to determine the exact gal/min of the water pump.

$$\text{mean 20 gal} - \text{mean 15 gal} = \text{difference in means}$$

$$2340 - \text{mean 15} \frac{\text{gal}}{\text{min}} = \text{difference from 15 gal for stock pump}$$

$$\frac{\text{difference from 15 gal/ min for stock pump}}{\text{difference in means}}$$

$$= \text{fraction between 15 and 20 gal/ min}$$

$$2876.3 - 2166.5 = 709.8$$

$$2340 - 2166.5 = 173.5$$

$$\frac{173.5}{709.8} = .244$$

$$(.244 * 5) + 15 = \text{REAL STOCK PUMP FLOW RATE} = 16.22 \text{ GAL/MIN}$$

This data from the chart above was also plotted in Excel and a trend line was used in order to curve fit the data and the following equation for fit was found as shown:

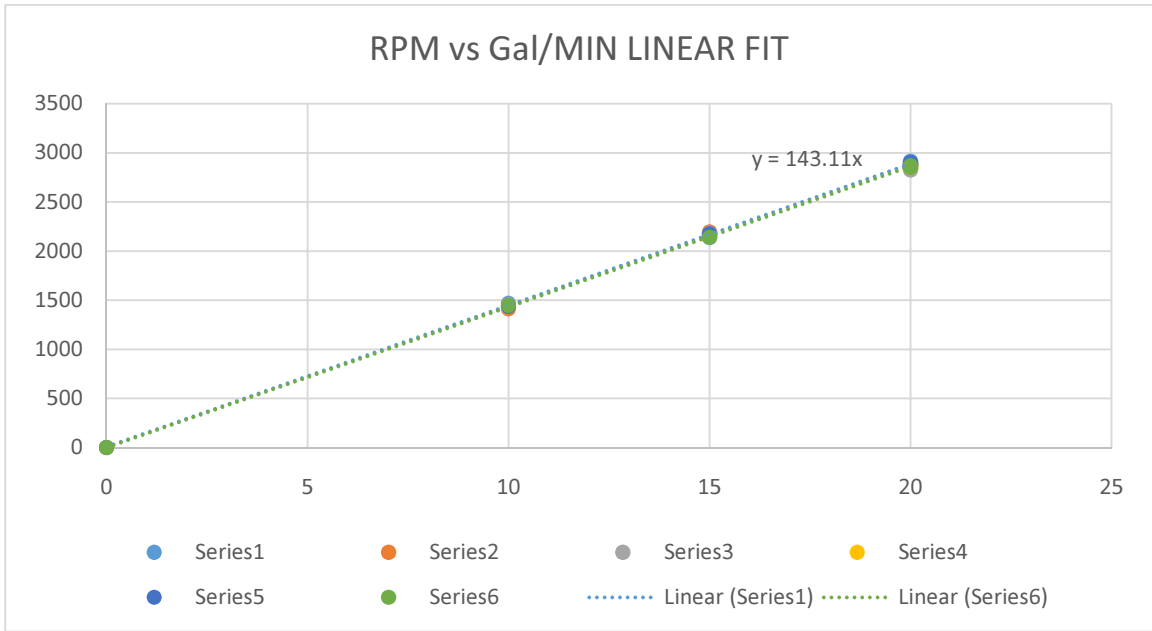


Figure 16: CURVE FIT DATA OF FLOW RATE VS WATER PUMP RPM

RPM is represented on the Y axis and GAL/Min on the X-axis. As can be seen there is a linear estimated relationship between the two variables. Using the equation $Y = 143.11 * X$ we would obtain a value at 2340 RPM to be 16.35 gal/min as the estimated stock pump power. This is only 0.8% different from the calculated flow rate of 16.22 gal/min so the estimation is extremely accurate and can be used as a representation of flow vs. RPM.

With this knowledge, the values for the modified 12% and 24% pulleys would increase speed to 18.31 gal/min and 20.27 gal/min, which based upon our first round of FLUENT modeling both showed substantial progress and vector movement in the point

in question. Following this data collection, new CFD flow data was calculated for 16.35, 18.31 and 20.27 gal/min as shown in Appendix D. These were the flow fields which would be predicted for the stock crankshaft pulley with the 12% and 24% speed reduction pulleys. Based upon initial FLUENT data at 17.5 gal/min there had appeared to be sufficient vector increase to cause adequate cooling and certainly at nearly 20 gal/min we will have more than substantial vector cooling motion available to mitigate the hot spot issue on the #4 cylinder.

TEST RESULTS

The engine was re-assembled utilizing the pulley which increased the water pump speed by 12%. The motor was run under identical conditions as previous work. The results from running the motor with the 12% larger flow rate were as follows:

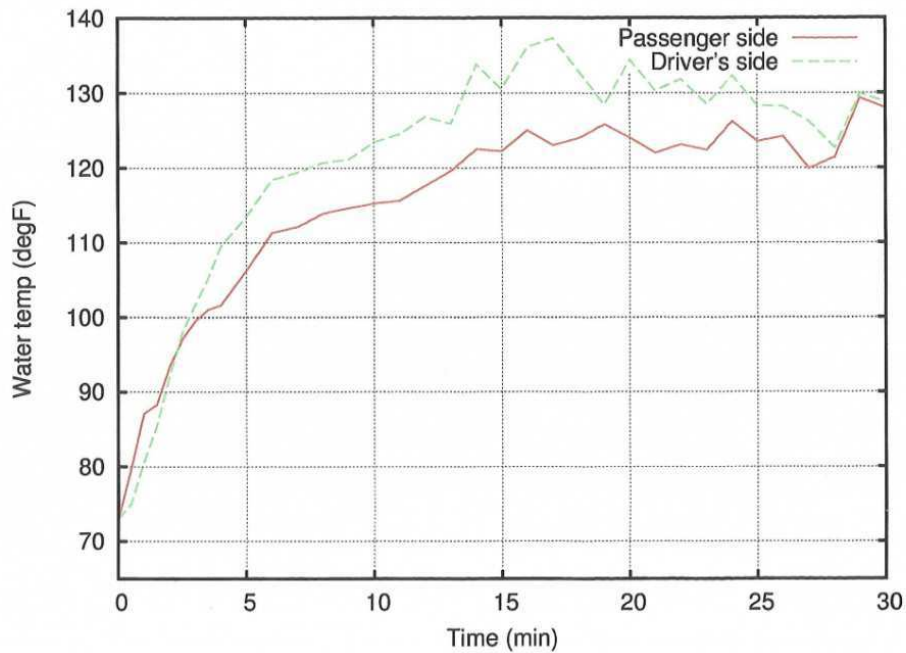


Figure 17: RECORDED WATER TEMP OF THE TWO SIDE OF THE CYLINDER BLOCK VS TIME

#time(min)	Pass_side	Driv_side
0	73.0	73.0
0.5	79.7	75.0
1	87.1	80.6
1.5	88.3	85.4
2	93.4	92.1
2.5	97.1	98.0
3	99.5	101.7
3.5	101.0	105.2
4	101.6	109.5
5	106.2	113.4
6	111.3	118.4
7	112.1	119.4
8	113.9	120.7
9	114.6	121.1
10	115.2	123.4
11	115.6	124.5
12	117.6	126.8
13	119.6	125.9
14	122.5	133.8
15	122.2	130.5
16	125.0	136.1
17	123.0	137.3
18	124.0	132.8
19	125.8	128.4
20	124.0	134.4
21	122.0	130.3
22	123.1	131.8
23	122.4	128.5
24	126.2	132.3
25	123.5	128.3
26	124.2	128.2
27	119.9	126.2
28	121.4	122.7
29	129.3	129.9
30	128.0	128.8

Figure 18: RECORDED WATER TEMPERATURE VS TIME OF PASSENGER AND DRIVERS SIDE THERMOCOUPLES

From the results it was apparent a substantial improvement in thermocouple temperature compared to previous work. Whereas the peak temperature reached 193.4 °F in 4 minutes in the previous work, the test results showed only 101.6 °F in the same time period. The maximum temperature reached by the passenger side hot spot location was 129.3 °F, well below an approach to boiling. From the chart we can also see that the passenger's side coolant temperatures were lower than that of the driver's side, which is contrary to the results of previous work. This suggests that the flow pattern behavior and development to the passenger side was indeed changed with the increase in water pump speed. For this reason, the 24% pulley was not tested as it would have most likely only

increased negatively the temperature gradient between the passenger and driver side of the block. During the test process it was noted that during the majority of the test period the thermostat remained closed and when it did open it remained in that position for only a few seconds before closing again.

CHAPTER 5

DISCUSSION

The initial modeling and subsequent set of models for different pulley size were run under the condition that the thermostat was open on the engine. Testing of the motor showed that most of the time was spent with the thermostat closed. In order to identify a possible explanation as to the behavior of the test results, further FLUENT modeling was run with a speed of 1 gal/min as an estimation of the closed thermostat condition to identify if the flow pattern was indeed different while the thermostat is closed. As suspected an entirely different flow pattern emerged under the closed thermostat condition as shown below.

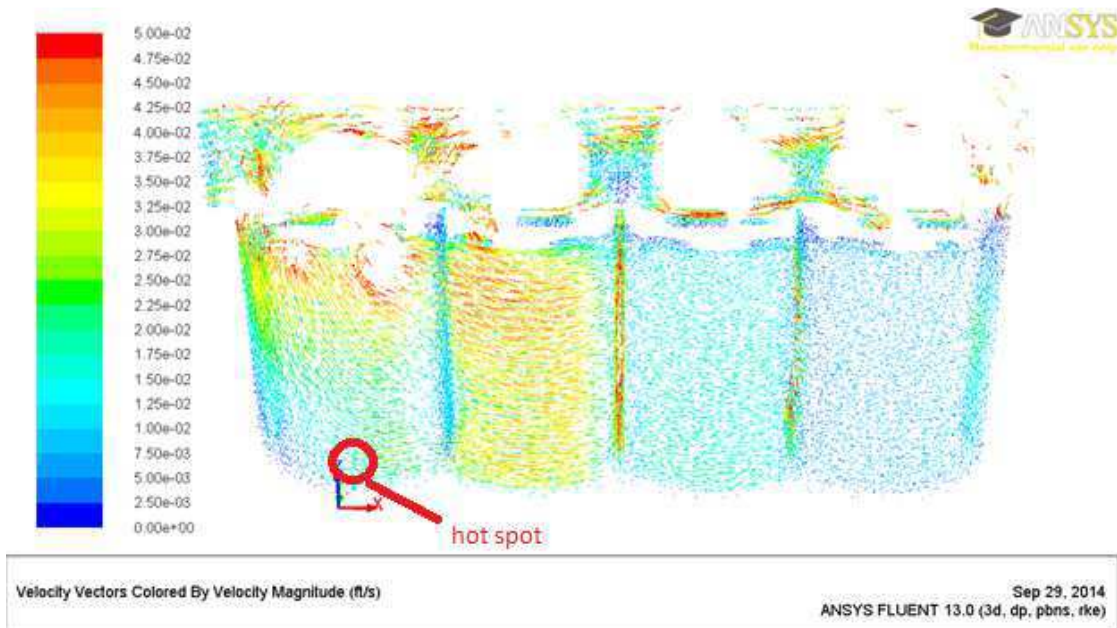


Figure 19: FLUENT FIGURE 1 GAL/MIN FLOW

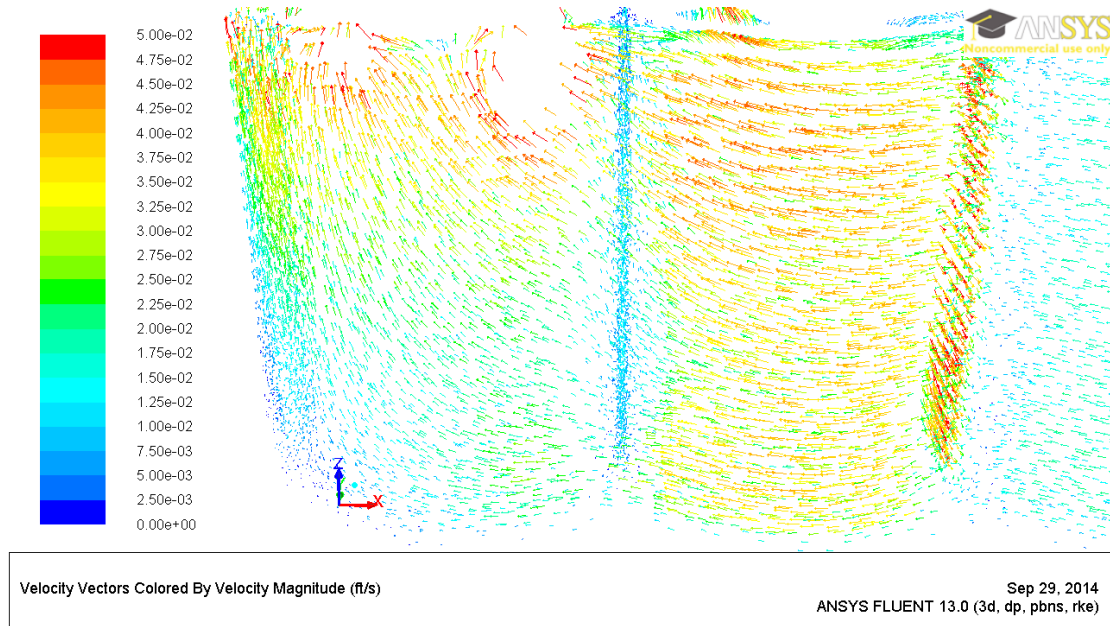


Figure 20: CLOSE UP OF HOT SPOT LOCATION UNDER 1 GAL/MIN FLOW

As can be seen in comparison to the results in APPENDIX B and figure 12 there is a completely different flow pattern achieved at low flow velocity conditions, i.e. when the thermostat is closed. The flow pattern moves the high velocity flow from between cylinders 1 and 2 to between cylinders 2 and 3 and the complex flow fields almost entirely disappeared. The flow represented in figure 12 by purple arrows that brings flow velocity past the hot spot is completely gone and as can be seen in the figures above the flow moves directly up to the top of the cylinder and out into the head, missing the hot spot location. As mentioned before, this flow pattern is of particular importance because the motor was operating under these flow conditions a majority of the time during testing. During testing a slow increase in the water inlet temperature gauge up to opening temperature was observed, followed by a swift drop indicating that the thermostat was only open for a few seconds at a time. This meant that there was a very short time period for the flow pattern to change from that of the 1 gal/min flow pattern which was at steady state to the higher 18.3 gal/min flow rate pattern. This short duration of thermostat

opening may not have allowed the flow pattern to ever reach the results shown in the higher flow rate CFD steady state analysis.

Fundamentally the reason that better cooling was achieved during this test was a direct result of faster water pump speed during both flow pattern conditions. Firstly, under closed thermostat conditions the flow rate would have already been 12% faster with the smaller pulley than the stock pulley, meaning the flow rate was already closer to the transition point to the steady state condition we initially modeled. Secondly, when the thermostat did open two things occurred: 1) A higher flow rate was already established and 2) The influx of flow was 12% greater than stock enabling a more rapid transit onto the more complete flow pattern with its high flow rate at the hotspot. It was noted before that the increase in flow rate would affect the entire flow field, and as such not only did the faster pump speed allow a possibility of developing the flow field depicted in purple arrows in figure 12 which cooled the hot spot, but it also enhanced the likelihood of an open thermostat steady state solution flow (depicted in green) in the front side of the block as well, which was seen as another potential high temperature area due to very low velocities.

Thus the increase in water pump speed achieved the result of increasing the flow at both open (preferential flow) and closed (non-preferential flow) conditions of the thermostat, allowing for enhanced cooling conditions at problematic areas in the passenger side of the engine block that had shown themselves in previous work. By increasing the water pump speed the water flow was able to get closer to the preferential flow field responsible for positive cooling of the high temperature hot spot areas of the engine.

FURTHER WORK

In order to more thoroughly understand the relationship between the thermostat, water pump speed and flow fields, dynamic modeling would need to be employed which does not look solely at the steady state flow conditions, but models the flow field change versus time. This would allow the determination of how quickly and to what extent the flow field changes from the non-preferential flow to the preferential flow within the engine when the thermostat opened and closed. This type of time dependent flow modeling would further explain the results achieved in this work and would aid in understanding optimal pulley speed for best operation. This work was beyond the scope of this thesis and would be a topic for future work.

APPENDIX A: CAD DESIGN ENGINE BLOCK

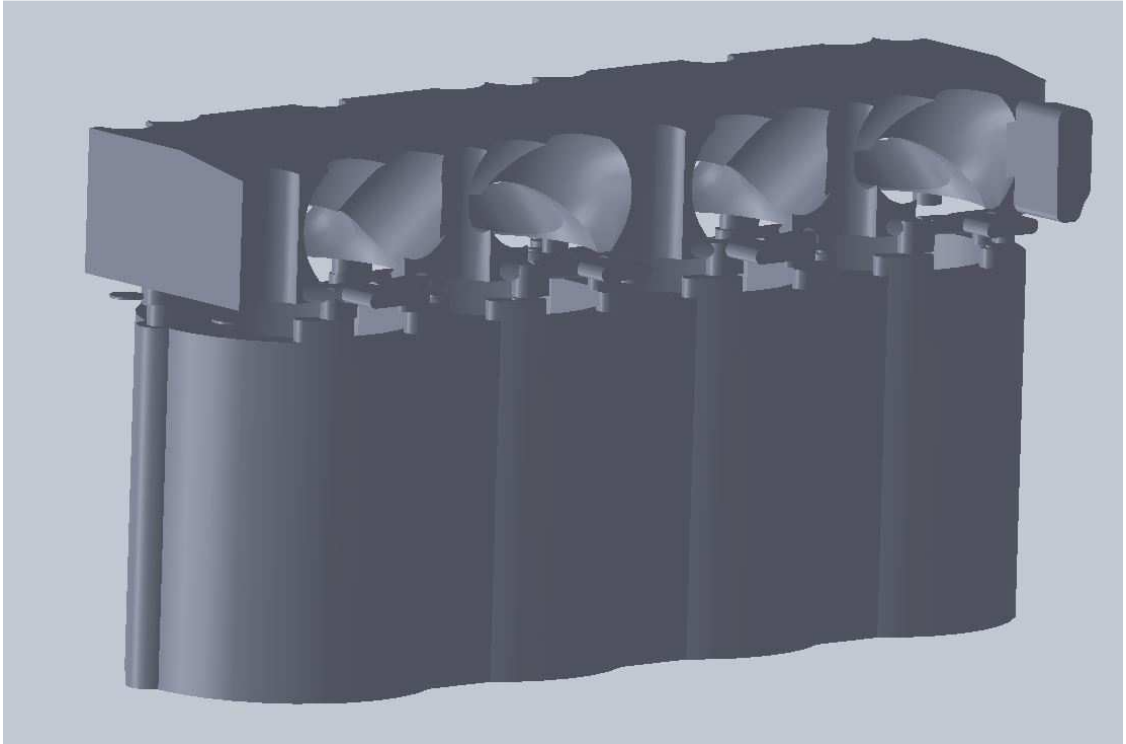


Figure A1: CAD MODEL PASSENGER SIDE

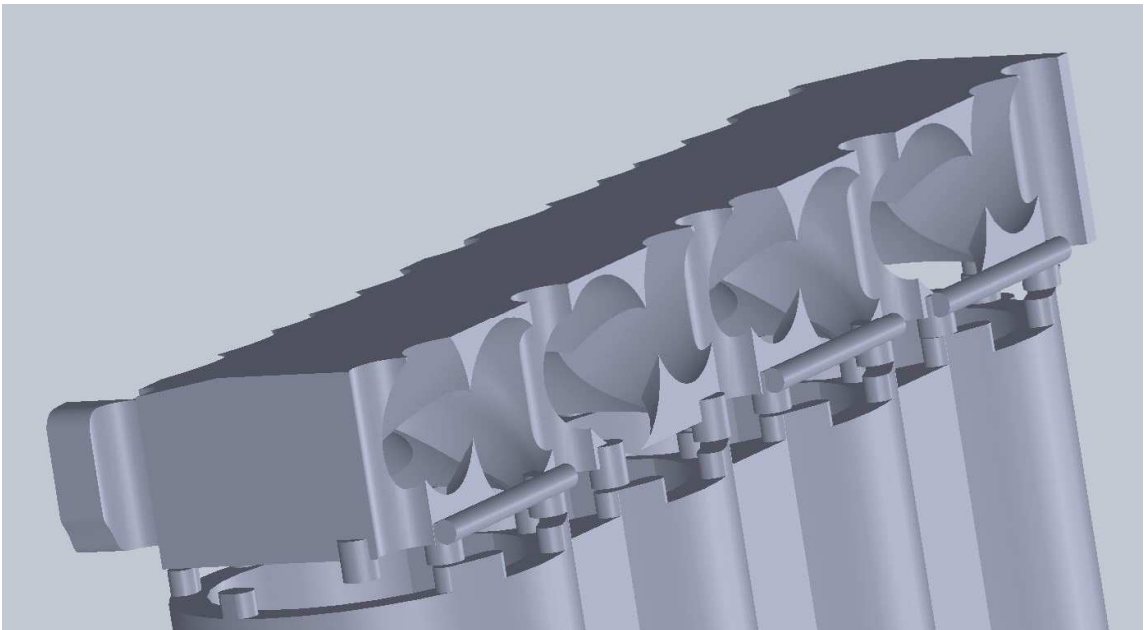


Figure A2: CAD MODEL DRIVERS SIDE

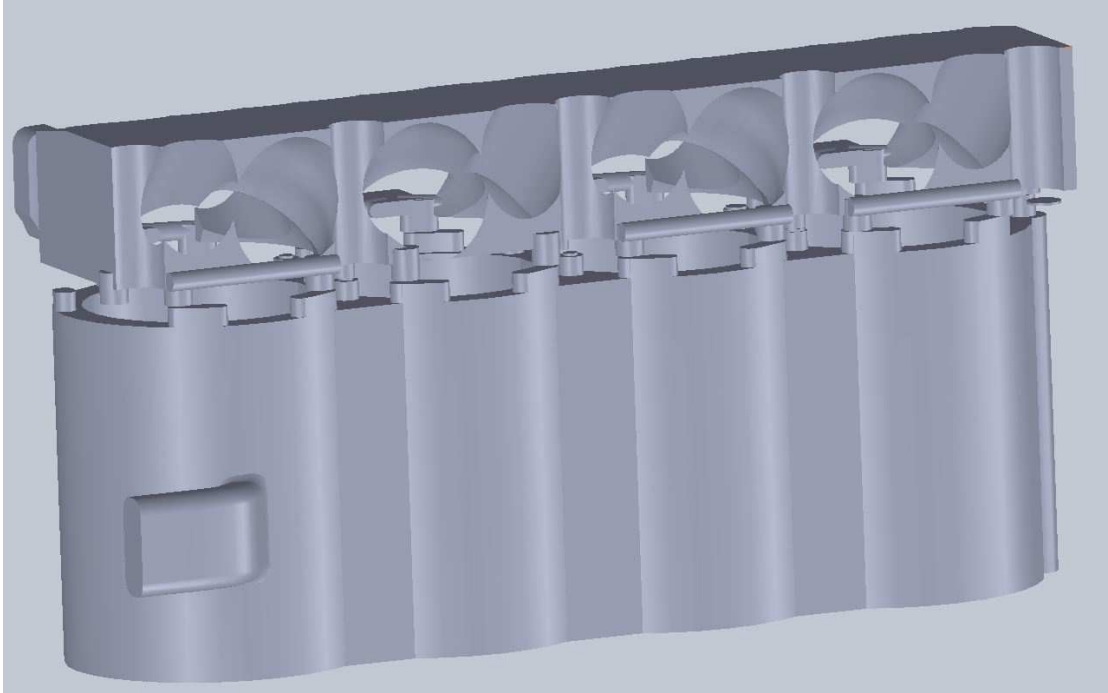


Figure A3: CAD MODEL FULL DRIVER'S SIDE

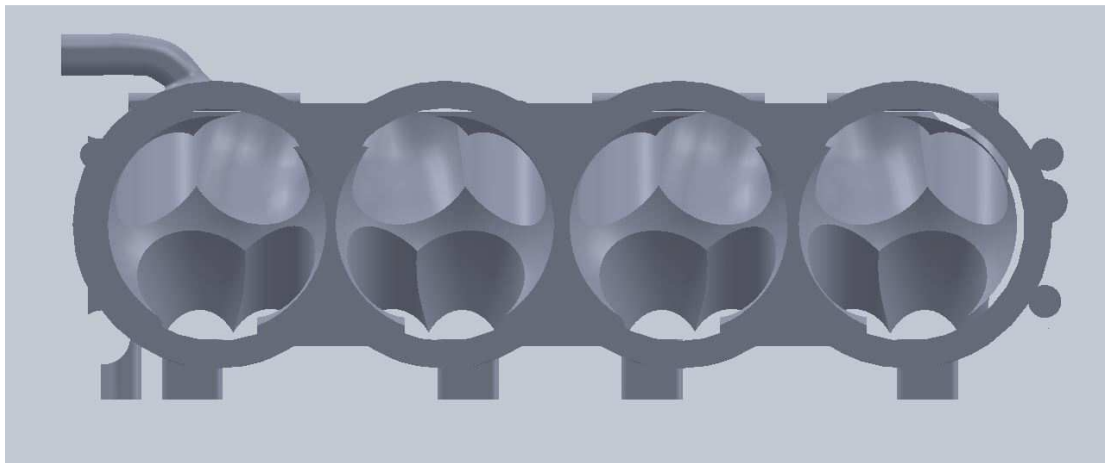
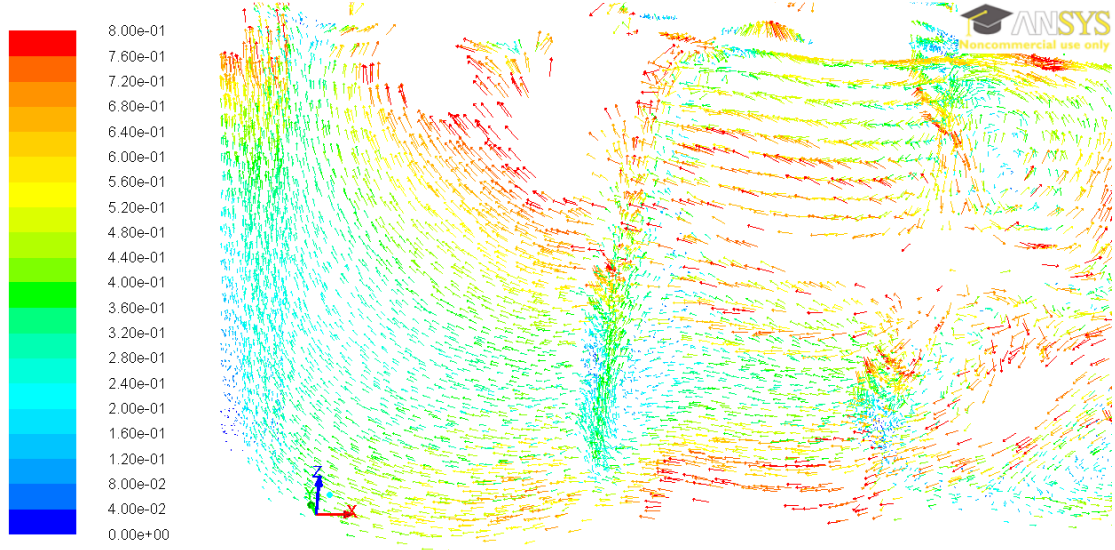


Figure A4: CAD MODEL BOTTOM SIDE VIEW

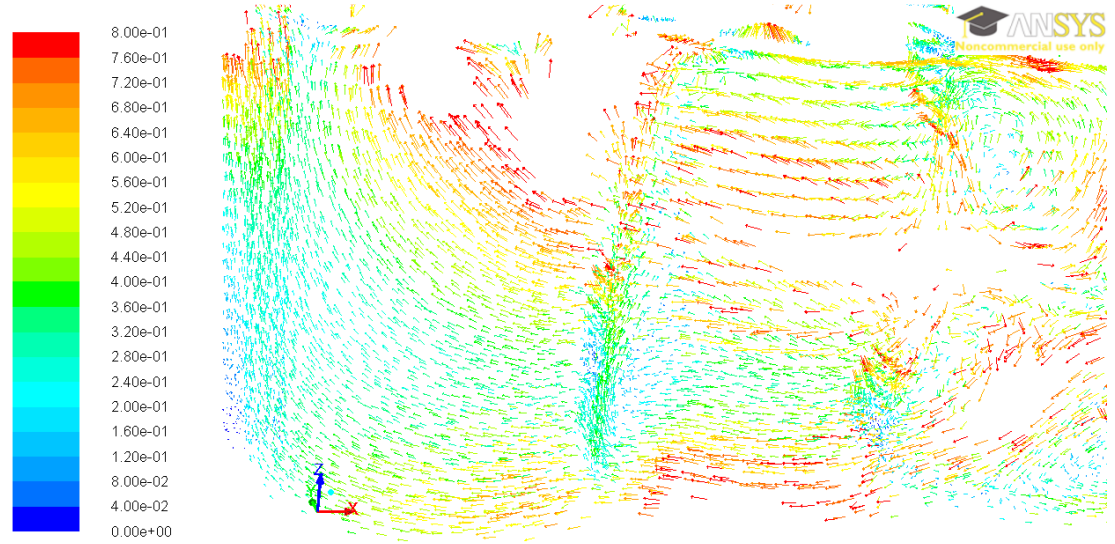
APPENDIX B: INITIAL FLUENT RESULTS



Velocity Vectors Colored By Velocity Magnitude (ft/s)

Sep 25, 2014
ANSYS FLUENT 13.0 (3d, pbns, rke)

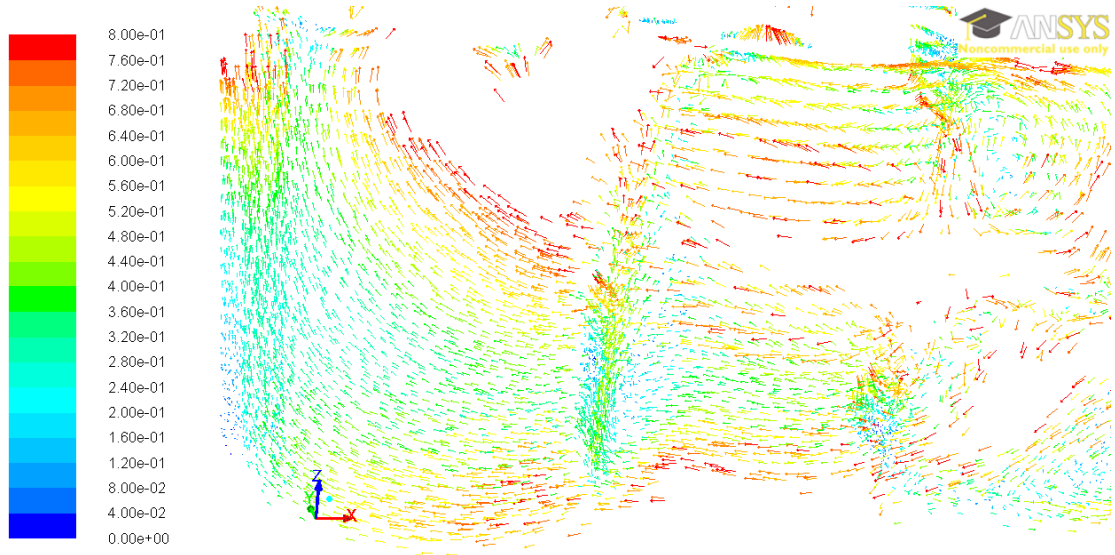
Figure B1: 15 GAL/MIN



Velocity Vectors Colored By Velocity Magnitude (ft/s)

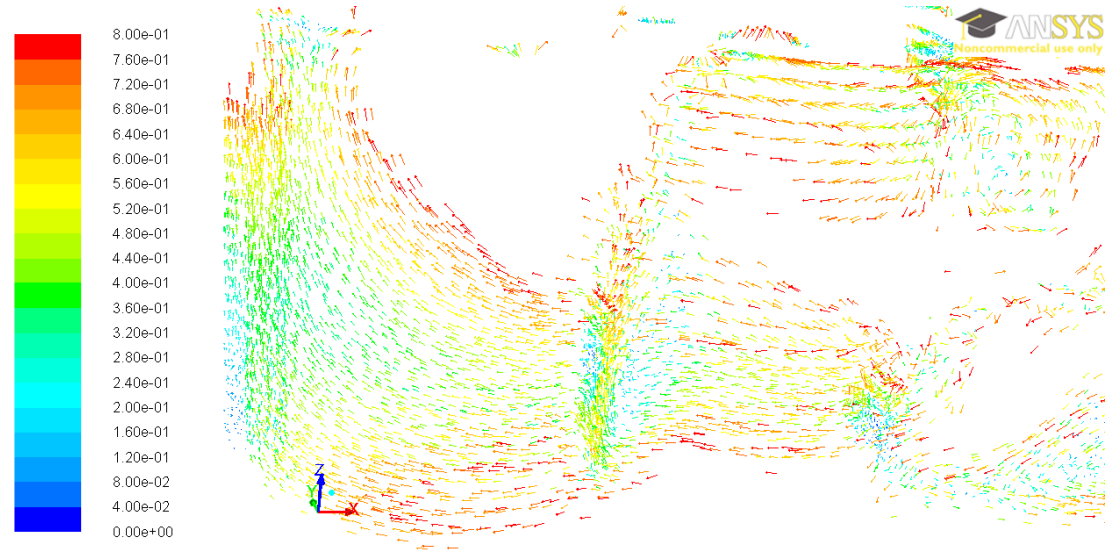
Sep 25, 2014
ANSYS FLUENT 13.0 (3d, pbns, rke)

Figure B2: 17.5 GAL/MIN



Velocity Vectors Colored By Velocity Magnitude (ft/s) Sep 25, 2014
ANSYS FLUENT 13.0 (3d, pbns, rke)

Figure B3: 20 GAL/MIN



Velocity Vectors Colored By Velocity Magnitude (ft/s) Sep 25, 2014
ANSYS FLUENT 13.0 (3d, pbns, rke)

Figure B4: 25 GAL/MIN

APPENDIX C: PULLEY DESIGN IN CAD

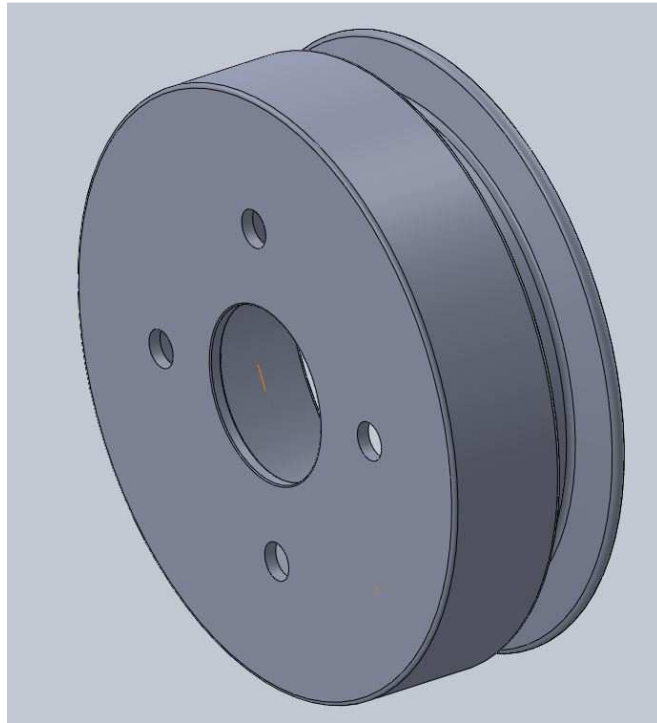


Figure C1: PULLEY CAD BACK SIDE

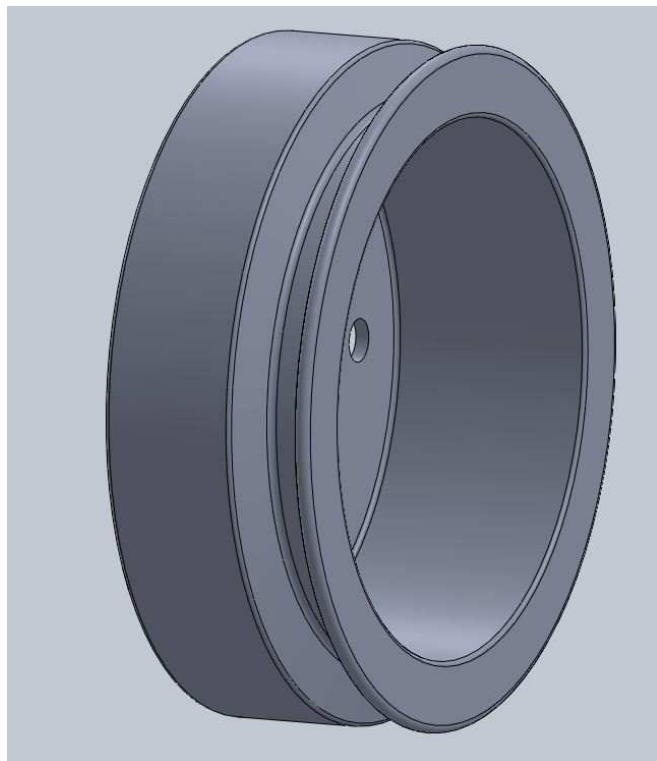


Figure C2: PULLEY CAD FRONT SIDE

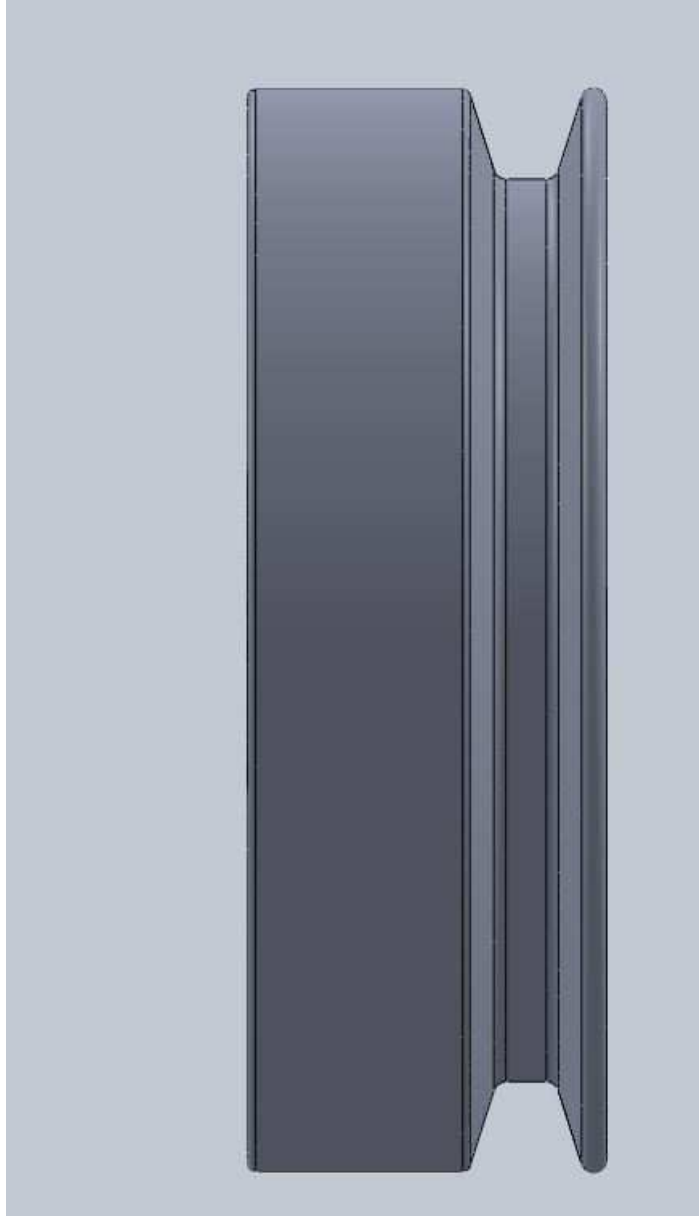


Figure C3: PULLEY CAD SIDE VIEW

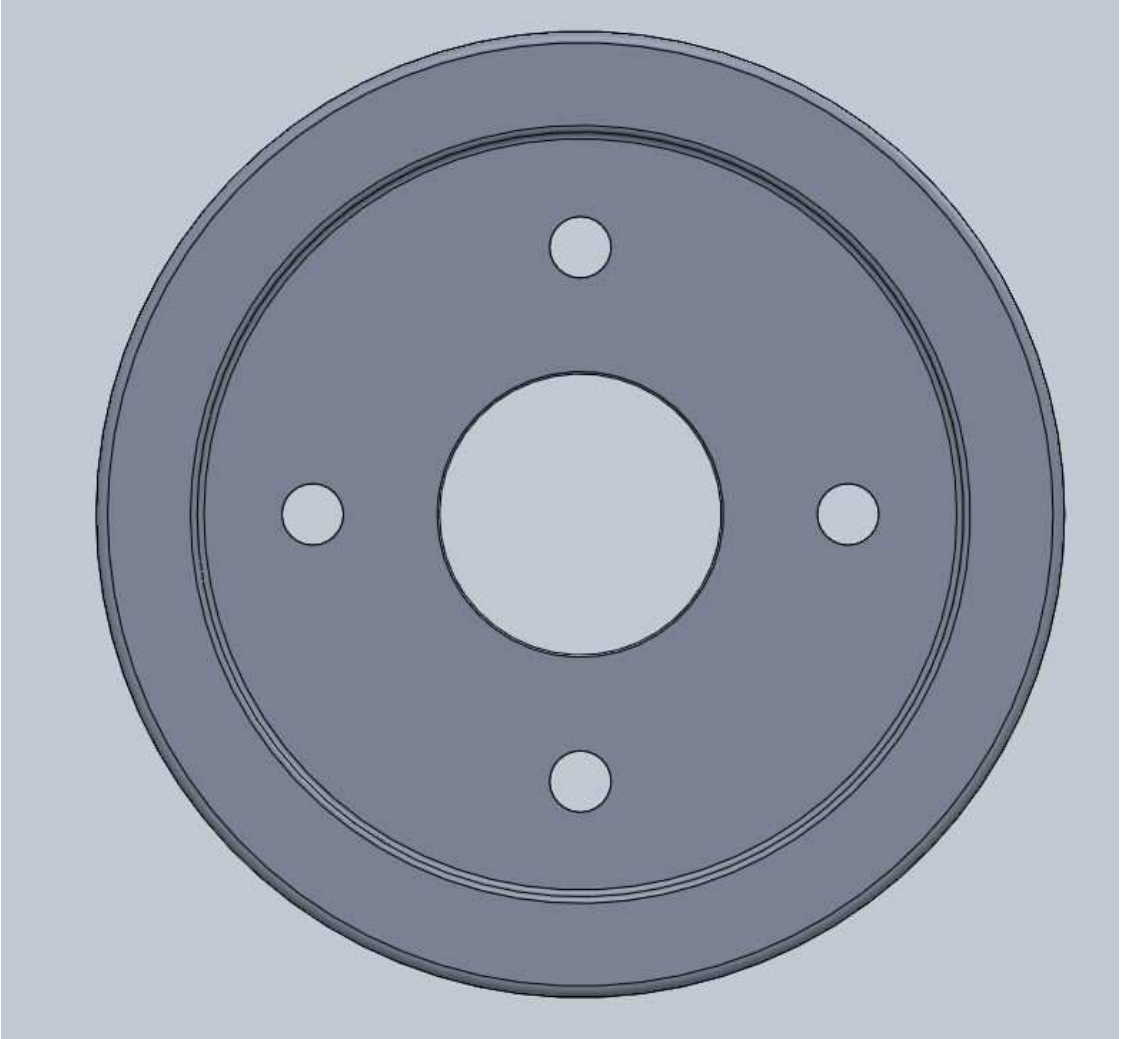


Figure C4: PULLEY CAD BACK VIEW DEAD ON

APPENDIX D: FLUENT FIGURES FOR ACTUAL FLOW RATES

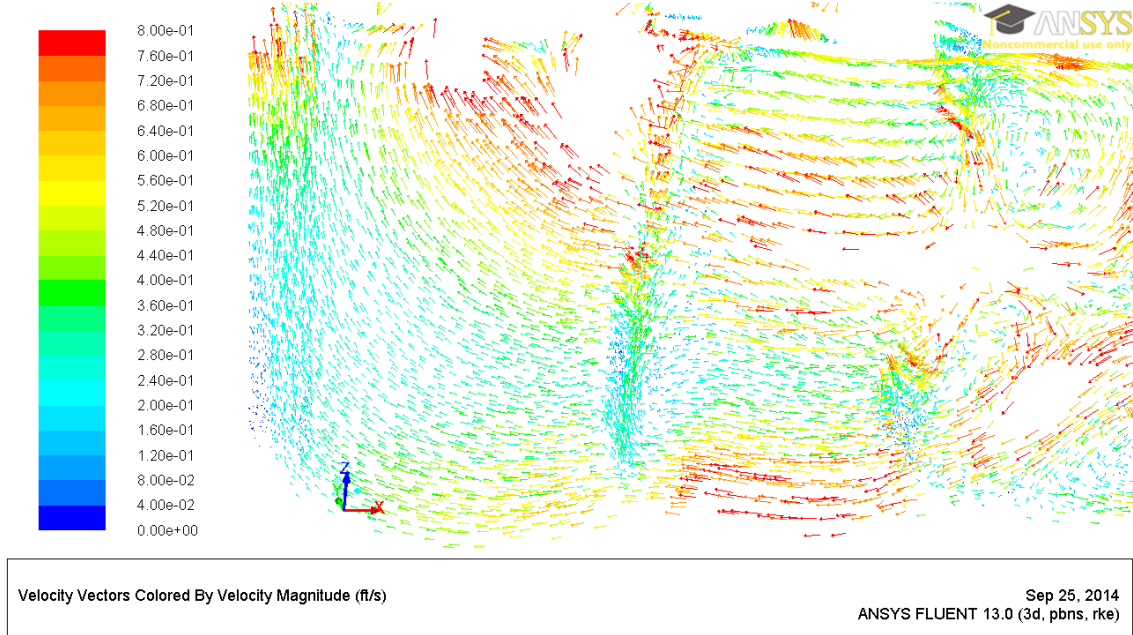


Figure D1: 16.35 GAL/MIN

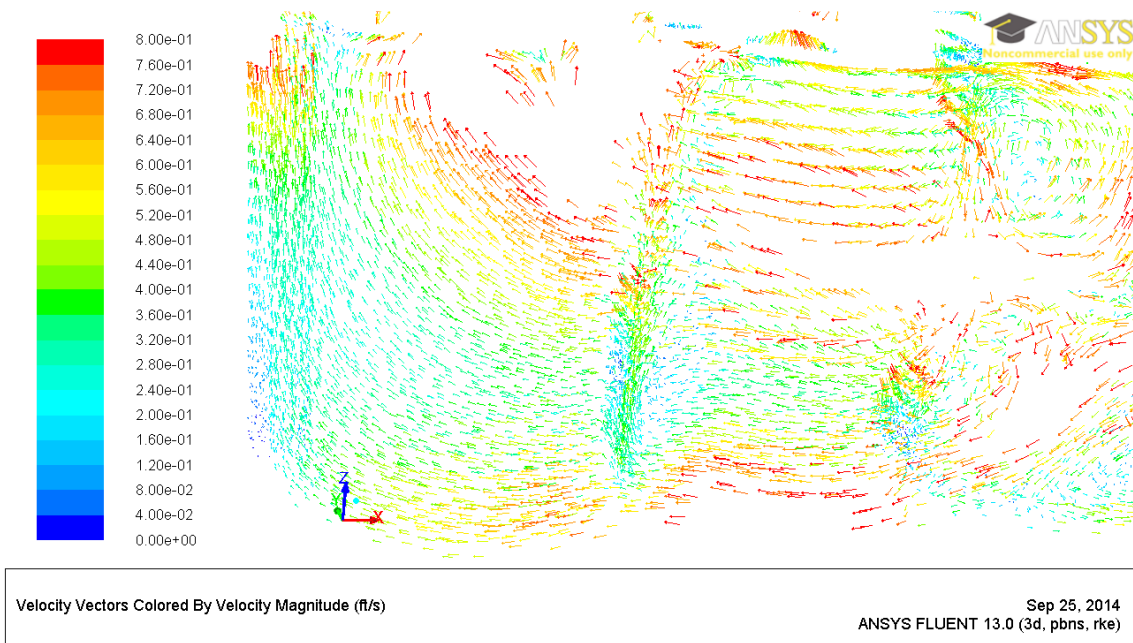
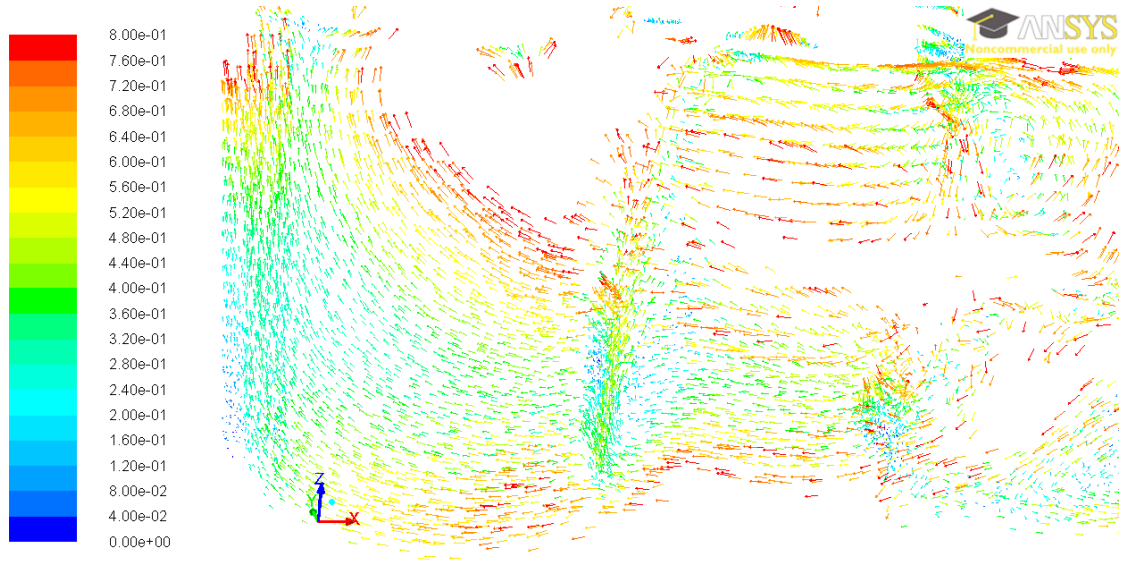


Figure D2: 18.32 GAL/MIN



Velocity Vectors Colored By Velocity Magnitude (ft/s) Sep 25, 2014
ANSYS FLUENT 13.0 (3d, pbns, rke)

Figure D3: 20.27 GAL/MIN

References

- [1] Oliver Jordan. Feasibility study of a low heat rejection generator set engine. Thesis. University of Miami. 2013

- [2] Richard Stone. Introduction to Internal Combustion Engines. Third Edition. 1999.

- [3] Irvin Glassman. Combustion. Second Edition. 1987.

- [4] Hasitha Samarajeewa. Design of 1.6 Liter Genset Engine. Thesis. University of Miami. 2011

- [5] Paul Robert Trumpler. Design of film Bearings. 1966.

- [6] Jorge Martins, Senhorinha Teixeira, and Stijn Coene. “Design of an Inlet Track of a Small I.C. Engine for Swirl Enhancement”. INTERNATIONAL CONGRESS OF MECHANICAL ENGINEERING, 20, Gramado, Brazil, 2009 – “Proceedings of COBEM 2009”. [Rio de Janeiro] : ACBM, 2009.